International Journal of Biological Macromolecules 259 (2024) 129296

Contents lists available at ScienceDirect

International Journal of Biological Macromolecules

journal homepage: www.elsevier.com/locate/ijbiomac

Self-assembly and hydrogelation of a potential bioactive peptide derived from quinoa proteins

Lirong Cheng [a], Luis M. De Leon-Rodriguez [b], Elliot Paul Gilbert [c,d], Trevor Loo [e], Ludwig Petters [f], Zhi Yang [g,*]

[a] Riddet Institute, Massey University, Palmerston North 4442, New Zealand
[b] School of Chemical Sciences, The University of Auckland, Auckland 1010, New Zealand
[c] Australian Centre for Neutron Scattering, Australian Nuclear Science and Technology Organisation, Locked Bag 2001, Kirrawee, NSW, Australia
[d] Centre for Nutrition and Food Sciences, Australian Institute for Bioengineering and Nanotechnology, The University of Queensland, Brisbane, QLD 4072, Australia
[e] BioProtection Aotearoa, School of Natural Sciences, Massey University, Palmerston North 4442, New Zealand
[f] School of Natural Sciences, Massey University, Palmerston North 4442, New Zealand
[g] School of Food and Advanced Technology, Massey University, Auckland 0632, New Zealand

ARTICLE INFO

Keywords:
Self-assembly
Fibrillar hydrogels
Quinoa proteins
Protofibrils
Secondary structures
Nanostructures
Rheology

ABSTRACT

In this work the identification of peptides derived from quinoa proteins which could potentially self-assemble, and form hydrogels was carried out with TANGO, a statistical mechanical based algorithm that predicts β-aggregate propensity of peptides. Peptides with the highest aggregate propensity were subjected to gelling screening experiments from which the most promising bioactive peptide with sequence KIVLDSDDPLFGGF was selected. The self-assembling and hydrogelation properties of the C-terminal amidated peptide (KIVLDSDDPLFGGF-NH_2) were studied. The effect of concentration, pH, and temperature on the secondary structure of the peptide were probed by circular dichroism (CD), while its nanostructure was studied by transmission electron microscopy (TEM) and small-angle neutron scattering (SANS). Results revealed the existence of random coil, α-helix, twisted β-sheet, and well-defined β-sheet secondary structures, with a range of nanostructures including elongated fibrils and bundles, whose proportion was dependant on the peptide concentration, pH, or temperature. The self-assembly of the peptide is demonstrated to follow established models of amyloid formation, which describe the unfolded peptide transiting from an α-helix-containing intermediate into β-sheet-rich protofibrils. The self-assembly is promoted at high concentrations, elevated temperatures, and pH values close to the peptide isoelectric point, and presumably mediated by hydrogen bond, hydrophobic and electrostatic interactions, and π-π interactions (from the F residue). At 15 mg/mL and pH 3.5, the peptide self-assembled and formed a self-supporting hydrogel exhibiting viscoelastic behaviour with G' (1 Hz) ~2300 Pa as determined by oscillatory rheology measurements. The study describes a straightforward method to monitor the self-assembly of plant protein derived peptides; further studies are needed to demonstrate the potential application of the formed hydrogels in food and biomedicine.

1. Introduction

In recent years, self-assembling and gel-forming peptides have gained paramount attention because of their ability to form a wide range of nanostructures including tubes, bundles, fibrils, micelles, and vesicles as well as potential intrinsic bioactivities such as antioxidant and antibacterial properties [1,2]. Due to their excellent biodegradability and biocompatibility as well as the environmentally responsible nature (e.g., temperature and pH), hydrogels that are formed from the self-assembly of peptides have found a vast number of applications in food encapsulation [3], drugs delivery [4], and tissue engineering [5,6]. Despite the extensive studies in characterisation and applications of peptide hydrogels, the prediction and design of peptides that can form hydrogels is still one of the largest challenges in this field [7], which has resulted in only a handful of experimentally and/or computationally demanding methods (using molecular dynamics simulations or machine learning methods and extensive peptide libraries) applicable to unveil peptide hydrogels no longer than four amino acids [8,9]. As a result, new peptide

* Corresponding author.
E-mail address: z.yang2@massey.ac.nz (Z. Yang).

https://doi.org/10.1016/j.ijbiomac.2024.129296
Received 29 November 2023; Received in revised form 25 December 2023; Accepted 5 January 2024
Available online 9 January 2024

gelators are usually found by accident or by modifying existing synthetic ones [10].

Identification of self-assembling peptides from food protein sources has gained increased popularity given some unique advantages [11]. First, peptides obtained from food protein hydrolysates are generally recognized as safe (GRAS) with a high biodegradability and biocompatibility profile [12,13]. Second, a large number of peptides derived from food protein hydrolysates have shown a wide spectrum of bioactivities including antidiabetic, inhibitors of cholesterol esterase, antioxidant, and antimicrobial activity, to name a few [14]. These factors establish food proteins as a promising resource for finding potential self-assembling peptides. However, research in this area is still in its infancy. Previous studies have reported the identification of peptide mixtures derived from enzymatic/acid hydrolysis or fermentation of food proteins, such as whey proteins [15], ovalbumin [16], and potato proteins [17], that can self-assemble into nanostructures or form aggregates and gels; however, the identification and characterisation of single peptide sequences derived from food proteins has been less scrutinized.

In a recent study conducted by Pugliese, Bartolomei, Bollati, Boschin, Arnoldi and Lammi [10], two food bioactive peptides isolated from the hydrolysis of soybean glycinin and lupin β-conglutin (namely IAVPTGVA and LTFPGSAED respectively) have been functionalised with a self-assembling peptide RADA16 to improve their gel forming capabilities. The results demonstrated that attaching either peptide to the *N*-terminal of RADA16 could significantly increase the gel strength (storage modulus *G'*) of the resultant biofunctionalized peptide relative to that of the food bioactive peptides. In another study, the same group reported that the gel strength of a lupin-derived peptide LNALEPDNTVQSEAGTIETWNPK hydrogel was significantly enhanced via an *N*-terminal biotinylated oligoglycine tag [18]. However, to the best of our knowledge, self-assembly and gelation behaviour of single peptide sequences derived from plant proteins without any modifications have not been identified and studied.

In this respect it is important to highlight that the simple identification of aggregation-prone peptide sequences that can form β-sheets and further assemble into various assembles, such as fibrils, nanotubes, and micelles is readily available via in-silico prediction tools [11] such as TANGO [19], AGGRESCAN [16], and WALTZ [20]. Furthermore, one can posit that aggregation-prone sequences can potentially lead to formation of hydrogels given that the kinetic parameters required to achieve the metastable gelation state are identified [12].

Quinoa (*Chenopodium quinoa*) is a pseudocereal that originates from South America and has recently become one of the emerging protein sources due to its high protein content 12–23 % *w*/w [21]. Furthermore, quinoa proteins contain all nine essential amino acids, and various quinoa derived peptides demonstrate health-promoting activities such as the inhibition of dietary carbohydrate digestion thus beneficial for the reducing the risk of type II diabetes [22]. A previous study demonstrated that quinoa protein Alcalase hydrolysates could form self-assembled peptide-based hydrogels [23]. In the current work, a potential bioactive peptide derived from quinoa protein enzymatic hydrolysates likely to form hydrogels was identified by in-silico aggregation-prone peptide predictions. The structural characteristics of the corresponding hydrogel were studied by transmission electron microscopy (TEM) and small angle neutron scattering (SANS), and its mechanical properties were studied by oscillatory rheology. Circular dichroism (CD) was employed to study the changes that occur to the secondary structure of the peptide during self-assembly and hydrogelation. This investigation provides details in relation to the mechanisms of self-assembly and hydrogelation of a peptide derived from quinoa proteins, which could be useful for their potential applications across a range of food and non-food areas.

2. Materials and methods

2.1. Materials and chemicals

The Peptide KIVLDSDDPLFGGF-NH_2 (Lys-Ile-Val-Leu-Asp-Ser-Asp-Asp-Pro-Leu-Phe-Gly-Gly-Phe-NH_2) (abbreviation: KF) (purity >95 %) was purchased from GL biochemical (Shanghai) Ltd. (Shanghai, China). HCl and NaOH were obtained from Sigma Aldrich (Auckland, New Zealand). Milli-Q water was used to preparate samples throughout the study. All chemicals and reagents used were of analytical grade.

2.2. Preparation of peptide solution and hydrogel

Peptide solutions were prepared by dissolving a certain amount of peptide powder into pure Milli-Q water. To achieve the desired final pH values (2, 3.5, 7.0, and 11.0), a weighed amount of peptide powder was dissolved in aqueous HCl or NaOH solutions based on the process reported by Castelletto and Hamley [24]. The final pH of the peptide solutions was measured with a HALO Bluetooth wireless pH electrode (Hanna Instruments, USA).

2.3. In silico analysis of peptide self-assembly and hydrogelation potential

A literature search of amino acid sequences of quinoa protein derived peptides, determined by liquid chromatography with tandem mass spectrometry (LC-MS/MS) analysis and reported the previous 5 years was performed. The β-sheet aggregation propensity (AGG score), which indicates the β-sheet aggregation propensity, of the collected peptide sequences either in the natural form or capped (*N*-terminal protected with the acetyl group or amidated at the C-terminal) was subsequently calculated using the algorithm TANGO (http://tango.crg.es/) [19,25,26] at pH 7, 25 °C with ionic strength of 100 mM and peptide concentration of 10 mM.

2.4. Circular dichroism (CD)

CD spectra of a set of peptide solution samples with different concentrations and pHs were recorded using a Chirascan V100 CD spectrometer (Applied photophysics, United Kingdom) with a 0.1 mm quartz cell (Hellma analytics, Germany). For ambient temperature experiments, the spectra were collected at 20 °C scanning from 260 nm to 180 nm with a step size of 0.5 nm. Temperature ramp experiments were conducted by increasing the temperature from 20 °C to 75 °C and then decreased to 20 °C in 5 °C steps with a 5 min equilibration time and data collection time of 2 min at each temperature. Vaseline was used to seal the edges of the quartz cell to prevent evaporation. Ten spectra were collected and the results were averaged before smoothing and background subtraction using Pro-data viewer software (version 4.4.1). CD measurements were performed in all peptide samples after ~1 h incubation at room temperature (~20 °C).

2.5. Negative staining transmission electron microscopy (TEM)

TEM imaging was conducted using a Tecnai G2 spirit BioTwin microscope (FEI, the Netherlands) operated at 200 kV. A sample of 20 μL of peptide solution was dropped onto a copper grid coated with a carbon support film and allowed to set for 1.5 min. Subsequently, the copper grid was immersed into a 1 % (*w/v*) uranyl acetate acid solution for staining. Afterwards, the stained samples were immersed in Milli-Q water for another 1.5 min to remove excess stain and dried with filter paper before observation. TEM images were obtained for all peptide samples after 1 day incubation at room temperature (~20 °C). The diameters of the individual fibrils were measured at ~15 positions for ~100 fibrils on the TEM micrograph of 15 mg/mL KIVLDSDDPLFGGF-NH_2 sample at pH 3.5 using the software programme Image J (NIH, Maryland, USA).

2.6. Small angle neutron scattering (SANS)

Time-resolved SANS measurements were performed in the QUOKKA SANS instrument at ANSTO, Sydney, Australia covering a *Q*-range of 0.003–0.4 $Å^{-1}$ [27,28]. The samples were prepared according to the procedure described in Section 2.2. Samples were injected into banjo cells (Hellma, Germany) and placed into a multi-position sample holder. All SANS measurements were performed at room temperature (~20 °C) and the self-assembly kinetics were followed for ~24 h. The following instrumental configurations were used: (i) source-to-sample (SSD) = sample-to-detector distance (SDD) = 20 m, (ii) SSD=SDD = 8 m and (iii) SSD = 4 m and SDD = 1.3 m with 300 mm detector offset for the latter, using a wavelength, λ, of 5 Å with 10 % resolution; an additional focussing optics configuration (iv) with the same SSD and SDD as in (i) was used to extend the low *Q* accessible to Q_{min} with a λ of 8.1 Å with 10 % resolution. *Q* is the magnitude of the scattering vector and is equal to $(4\pi/\lambda)\sin(\theta)$, and where 2θ is the scattering angle. For all configurations, the sample aperture of 12.5 mm was used. Neutron source aperture of 50 mm was use for (i), (ii) and (iii) and 30 mm for (iv). The data were reduced and merged using the Igor Pro software (Wavemetrics, USA) following a standard procedure. All the SANS data were background subtracted with 100 % H_2O.

2.7. SANS data analysis

SANS data analysis was performed using the Modelling II tool of the Irena SAS package incorporated in a commercial Igor Pro 8.0 software (Wavemetrics, USA) [29]. A power law model (Eq. (1)) was used to fit the scattering data in the low *Q* regime ($Q < 0.006$ $Å^{-1}$).

$$I(Q) = aQ^{-n} \tag{1}$$

where *a* represents a scale factor and *n* is the power law exponent. In the mid-to-high *Q* regime ($0.006 < Q < 0.3$ $Å^{-1}$), data were modelled using a cylindrical form factor (P(Q)) with radius following a log-normal distribution, as indicated in Eq. (2) [30]:

$$p(Q) = \frac{Scale}{V_{cyl}} \int_0^{\pi/2} f^2(Q,\alpha) sin\alpha d\alpha$$

$$f(Q,\alpha) = 2(\rho_{cly} - \rho_{solv}) V_{cyl} j_0(QH\, cos\alpha) \frac{J_1(Qr\, sin\alpha)}{(Qr\, sin\alpha)}$$

$$j_0(x) = \frac{sin(x)}{x} \tag{2}$$

where V_{cyl} represents the volume of the cylinder. $J_1(x)$ is first order Bessel function, and α is the angle between cylinder axis and the scattering vector. H is the half length of the cylinder. ρ_{cyl} and ρ_{solv} are the neutron scattering length densities (SLDs) of the cylindrical scattering object and the surrounding solvent. During the modelling, the length of fibrils was fixed to an arbitrarily large value of 20,000 Å i.e. much less than the inverse of the minimum accessible instrumental *Q* and the SLD of the peptide fibrils and solvent (H_2O) were set as 1.9×10^{-6} $Å^{-2}$ and -0.56×10^{-6} $Å^{-2}$, respectively [31].

2.8. X-ray diffraction (XRD)

A 15 mg/mL peptide solution at pH 3.5 was prepared following the procedure described in Section 2.2. The peptide solution was left overnight at room temperature (~20 °C) to enable self-assembly. Aliquots of the peptide solution were then transferred into a 1.5 mL Eppendorf tube and dried at room temperature in a fume hood for 24 h. Finally, the dried samples were milled to powders with a pestle and mortar before mounting onto a sample holder. X-ray diffraction data were collected using a diffractometer (Bruker D8 Venture, Germany) with a copper radiation source at a wavelength of λ = 1.54 Å.

2.9. Rheological measurements

Small and large deformation rheological measurements were performed using a rotational TA DHR-3 stress-controlled rheometer (TA instruments, USA) equipped with a parallel plate geometry (20 mm diameter and 1 mm gap). Aliquots of the peptide solution (15 mg/mL, pH 3.5) were transferred onto the bottom plate using a pipette. To prevent evaporation during measurement, low viscosity mineral oil (M 5904, Sigma Aldrich, USA) was added around the edge of the geometry. The rheological characterisations were conducted according to the following protocol: (1) a time sweep measurement was conducted at 20 °C for 12 h using a fixed strain 0.5 % and frequency 1 Hz to monitor gelation kinetics; (2) at the completion of step 1, a frequency sweep measurement was conducted with the frequency ranging from 0.01 to 30 Hz at a constant strain 0.5 % to probe viscoelastic behaviour of peptide gels; and (3) finally, a strain sweep test was conducted with strain varied from 0.01 to 1000 % at a constant frequency 1 Hz in order to study large deformation rheological properties of the peptide gels. Both frequency sweep and strain sweep measurements were conducted at 20 °C. Temperature sweep measurements for 15 mg/mL, pH 3.5 KF sample were performed at a fixed strain 0.5 % and frequency 1 Hz over a heating-colling cycle between 20 °C to 90 °C at a rate of 1 °C/min.

3. Results and discussion

3.1. Prediction of hydrogelation potentials of quinoa derived peptides and preliminary gelation screening

The TANGO predicted β-sheet aggregation propensity (represented by the AGG score) of peptides derived from enzymatic hydrolysis of quinoa proteins reported in the literature is listed in Table S1. The TANGO calculation was performed on the peptides in their natural form (uncapped) and capped with protecting groups (acetyl or amide). A previous study demonstrated that the peptide capped with protecting groups could facilitate self-assembly and hydrogelation [32]. Peptides with AGG score ≥ 1 were considered to exhibit high β-sheet aggregation propensity [33]. As shown in Table S1, there were 24 peptides (either in its natural or terminal protected form) out of 210 peptides with AGG scores ≥1. Due to budget constraints, three of these peptides Ac-LSLGVAGSRPGFEG (LG), KIVLDSDDPLFGGF-NH_2 (KF), and RGAIVL-NH_2 (RL) were acquired. A simple tube-inversion test was performed for 15 mg/mL peptides at four pH values (2.0, 3.5, 7.0, and 11.0) demonstrating that only KF could form a self-supporting hydrogel under certain pHs. Therefore, the KF peptide was selected for further characterisation. Interestingly, a previous in-silico analysis study predicted that the KF peptide has a wide range of bioactivities including inhibition of α-glucosidase, dipeptidyl peptidase-IV and angiotensin I converting enzymes (Table S2) [22].

3.2. The effect of pH, peptide concentration and temperature on the secondary structure of the peptide during self-assembly

pH can have a significant impact on the self-assembly behaviour of the KF peptide in aqueous solution as it carries a few charged and pH sensitive amino acids such as Lys (basic) and Asp (acidic). As shown in Fig. S1, at a sufficiently high concentration (15 mg/mL), KF could form self-supporting hydrogels at acidic pHs (2.0 and 3.5). The hydrogel formed at pH 3.5 is transparent while the hydrogel formed at pH 2.0 is turbid. At neutral and alkaline pHs (7.0 and 11.0), no hydrogel was formed. This could be due to the fact that pH 3.5 is closer to the isoelectric point (PI) of the peptide (pI ~4.01), thus promoting aggregation and self-assembly [13]. Previous studies demonstrated that secondary structural transitions have a significant impact on the self-assembly and gelation behaviour of peptides. Circular dichroism (CD) is one of the most well-established and classically used techniques to characterise peptide secondary structure and has been used to detect the presence of

β-sheets including parallel and antiparallel β-strands in fibrillar peptide nanostructures [34,35]. Far-UV CD was therefore used to probe the secondary structural changes as a function of pH at three concentrations of KF: 2 mg/mL, 5 mg/mL, and 15 mg/mL (Fig. 1A, C, E). It can be clearly seen that secondary structures of KF peptides are considerably affected by the pH in a concentration dependent manner. At a lower concentration (2 mg/mL) and all pH values, KF showed an intense negative peak at around 203 nm (Fig. 1A), which is characteristic of a disordered random coil secondary structure [24]. In addition, a small peak dip at around 225 nm that corresponds to twisted antiparallel β-sheet structure [36] can be identified at pH 3.5 and pH 2.0, indicating the KF peptide formed a small portion of β-sheet secondary structure at the acidic pH. When the concentration was increased to 5 mg/mL (Fig. 1C), two prominent negative peaks appeared at around 205 nm and 226 nm for pH 7.0 and pH 11.0 respectively, suggesting the formation of α-helix secondary structure with increasing peptide concentration [36]. There is only one peak centred around 225 nm observed at pH 2.0, suggesting acidic pHs are more favourable for the formation of β-sheet-rich secondary structures. It has been suggested that pH adjustment could alter the net charge on peptide molecules thereby adjusting their aggregation propensity into intermolecular β-sheet structures [37,38]. When the pH was decreased close to the isoelectric point of the KF peptide (calculated to be pH 4.01 from https://pepcalc.com/), the net charge on the peptide molecule tends to be minimised. Therefore, molecular attraction dominates repulsions, potentially facilitating intermolecular association into β-sheet amyloid structures [1,39]. A similar finding has been reported in other pH dependent self-assembled peptide systems such as the coronavirus spike peptide RSAIEDLLFDKV [24] and α-synuclein [40]. When the KF peptide concentration was further increased to 15 mg/mL at all pHs (Fig. 1E), a single peak characterised by a minimum at 223–228 nm, representing a β-sheet secondary structure, was identified. However, the absolute peak intensity varied significantly, following the order of pH 2.0 > pH 3.5 > pH 11.0 > pH 7.0. These results indicate that at a sufficiently high concentration of KF peptide (15 mg/mL), the β-sheet rich secondary structures are established at all pHs with acidic pHs enabling a higher proportion of β-sheet structure. In addition, the CD negative peak shifted from ~230 nm at pH 7.0 and pH 11.0 to a lower wavelength ~ 265 nm at acidic pHs (Fig. 1E). The peak at acidic pHs also tended to be narrower than those at pH 7.0 and pH 11.0. This result indicates that acidic pHs enable the transition from antiparallel twisted β-sheet to well-defined β-sheet secondary structures [36].

Besides the impact of pH, the concentration dependency of KF self-assembly behaviour was also investigated. As shown in Fig. S1, at lower concentrations (2 and 5 mg/mL), no hydrogels were formed irrespective of pH. The evolution of KF peptide secondary structure as a function of concentration at four pHs were probed by CD and the results are shown in Fig. 1B, D, F, G. The concentration dependence of the CD spectra follows a similar trend at all pHs. Increasing concentration from 2 mg/mL to 5 mg/mL leads to a considerable reduction of the negative CD peak at ~200–205 nm (representing a random coil), progressive peak red-shift, and a concomitant emergence of another strong native CD peak at ~225–230 nm. More specifically, at 5 mg/mL, the CD spectra revealed two minima at around 208 nm and 225 nm for pH 3.5, and 206 nm and 228 nm for pH 7.0 and pH 11.0. These are characteristic of an α-helical conformation [36,41]. A broad band between 215 and 230 nm was observed for a sample at 5 mg/mL peptide concentration and pH 2 (Fig. 1B), which may arise from contributions of β-sheet and α-helix to the spectra [42]. The presence of a α-helical structure during peptide self-assembly at various concentrations was also observed in a previous CD study of the peptide IVD (also name Ac-LD_3) [43] and a fungal ribonucleoprotein (RNP) protein [44]. The α-helical secondary structure has been suggested to represent an intermediate oligomeric species that occurs during the transition from the unfolded native peptide to β-sheet-rich protofibrils [42,43]. Increasing the concentration further to 15 mg/mL leads to a transition to a single negative band at around at 225–230 nm accompanied by a substantial intensity enhancement. These findings suggest an increasing of β-sheet secondary structure upon increasing the peptide concentration. It has been proposed that the tendency of the peptides to self-assemble or form intermolecular β-sheet structures is strongly related to the peptide concentration [45]. At high concentrations, interactions between peptide molecules are more favourable due to closer contact, thus promoting the formation of strong intermolecular H-bonding and β-sheet secondary structures [36]. Similar observations have been found in previous CD studies of a hybrid polymer-peptide conjugate, PEG_8-$(FY)_3$ [45] and a biologically active peptide PEP-1 [36]. From the concentration dependent CD results, it can be inferred that the self-assembly of the KF peptide follows the major models proposed for amyloid formation, which describe the unfolded peptide firstly transiting to an α-helix-containing intermediate and then rearranging into β-sheet-rich protofibrils [46,47]. This finding also agrees well with the observation in Fig. S1 that no hydrogel is formed at lower concentration (2 and 5 mg/mL) and which could be attributed to low content of β-sheet secondary structure.

Temperature is another critical factor that could significantly affect the secondary structure transitions and self-assembly behaviour of peptides [36,48]. To study the effect of temperature, CD spectra were collected for peptide samples during heating (Fig. 2) and cooling (Fig. 3). At 2 mg/mL and all pHs, increasing temperature from 20 °C to 75 °C induced a progressive CD peak shift from around 200 nm to around 206 nm, and a concomitant enhancement in negative CD peak at around 225 nm. This clearly indicated that heating could facilitate the secondary structure transition from random coil to α-helix [36]. For the sample at 5 mg/mL in acidic pHs (pH 2.0 and pH 3.5), the negative peak at around 225 nm became dominant during heating, suggesting an increase in the content of β-sheet secondary structure [36]. Whereas at pH 7.0 and pH 11.0, there are two minima around ~205 nm and ~ 230 nm representing α-helix secondary structures at 20 °C. They progressively changed to a single broad peak at around ~225 nm during heating. This indicated the gradual transition from intermediate α-helix to β-sheet-rich structures at elevated temperatures; such behaviour has been reported in previous temperature-dependent CD studies on the LIVAGD peptide [43] and a myostatin precursor protein [42]. At 15 mg/mL for all pHs, the negative peak at around 225 nm increased strongly with an increase in temperature (1.5–3 folds depending on pH). This again suggested that heating could significantly promote formation of β-sheet secondary structure [49]. This effect may be explained by the fact that hydrophobic interactions are promoted by heat treatment, leading to closer contact between peptide molecules and the formation of strong intermolecular H-bonding and enhanced π-π interactions into stable conformations [36]. Alternatively, this lower critical solution temperature (LCST) behaviour could be attributed to improved facial β-sheet interstrand interactions as suggested by the increase in intensity of the β-sheet band observed in CD [50]. Furthermore, the peak shift from ~230 nm to ~226 nm was observed for the sample at 15 mg/mL, pH 7.0 and pH 11.0 during a temperature sweep from 20 °C to 75 °C. The shift in peak wavelength suggests that peptide molecular conformations and arrangements can be altered by an increase in temperature, leading to distortion of the β-sheet [48]. More specifically, this finding indicates that elevated temperatures could enable the transition of twisted β-sheet rich domains formed at room temperature (~20 °C) into strong and well-defined β-sheet structures representing a thermodynamically controlled state [36]. Similar observations have been reported in previous CD studies of a PEP-1 peptide [36] and a Gram-positive antibacterially active peptide $(KIGAKI)_3$-NH_2 [51].

To study if heating-induced secondary structural changes are reversible, CD spectra were also acquired for all peptide samples during cooling from 75 °C to 20 °C. As shown in Fig. 3, one can see that temperature-induced changes are (partially) reversible for all samples. To further understand the thermally reversibility of peptide self-assembly and secondary structure changes, the intensity of the peak at 226 nm reflecting the β-sheet content was plotted versus temperature

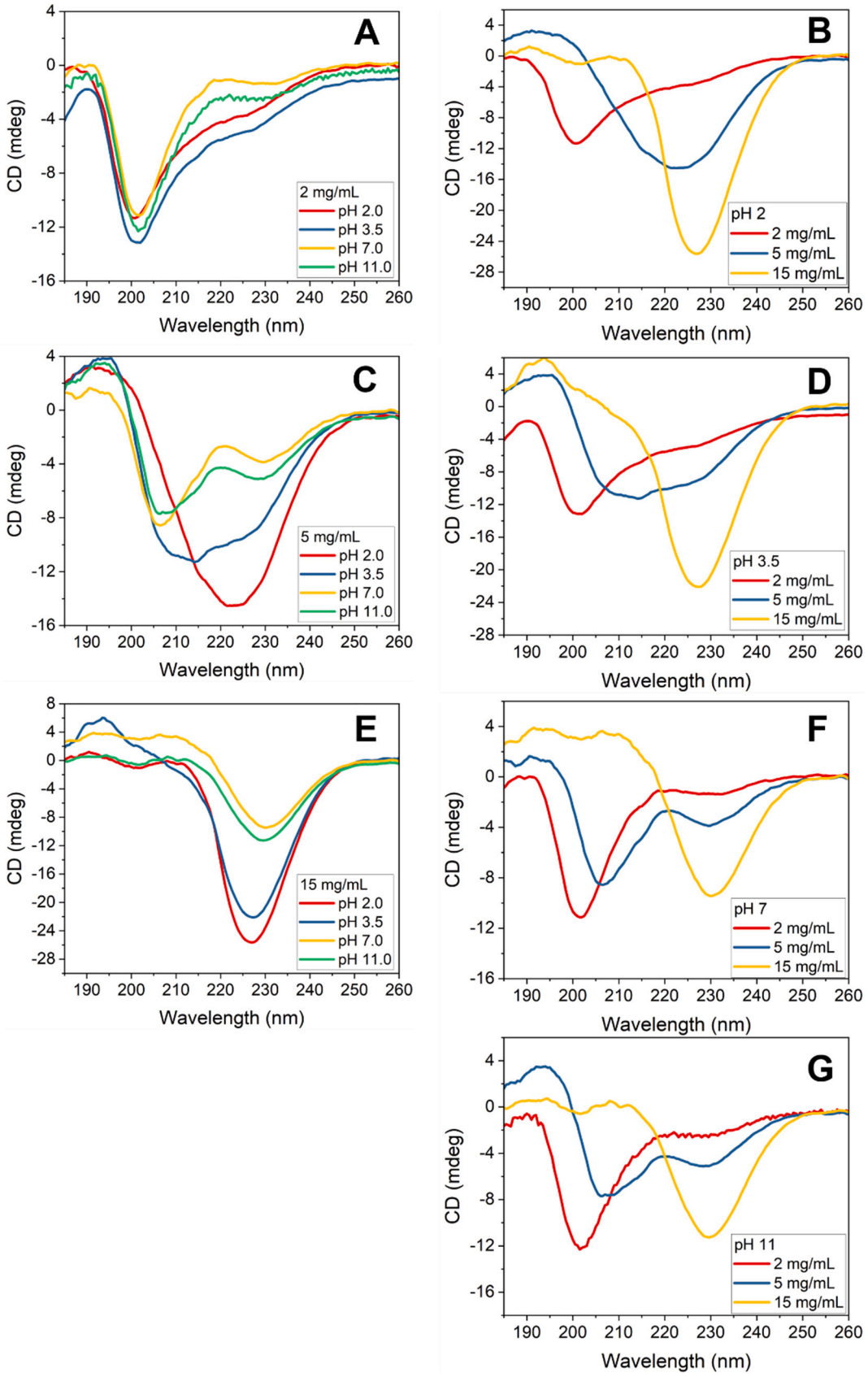

Fig. 1. pH-dependent CD spectra of KF peptide at (A) 2 mg/mL, (C) 5 mg/mL, and (E) 15 mg/mL; Concentration-dependent CD spectra of KF peptide at (B) pH 2.0, (D) pH 3.5, (F) pH 7.0, and (G) pH 11.0.

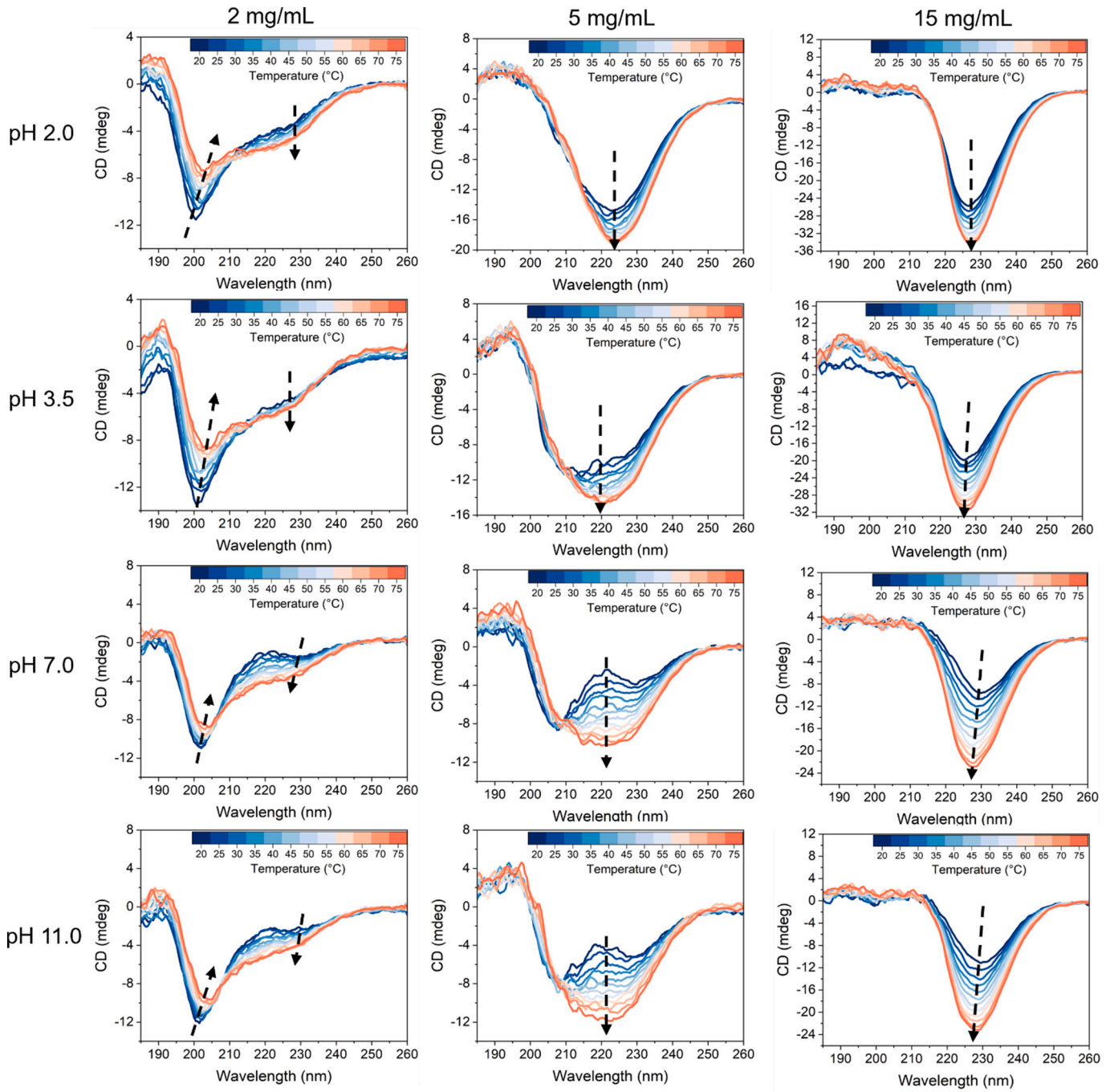

Fig. 2. Temperature-dependent CD spectra of KF peptide at various pHs (pH 2.0, pH 3.5, pH 7.0, pH 11.0) and concentrations (2 mg/mL, 5 mg/mL, and 15 mg/mL) when the temperature is increased from 20 °C to 75 °C. Arrows indicate the CD spectra change as the temperature increases.

during heating and cooling (Fig. 4). At low concentrations (2 mg/mL and 5 mg/mL) samples at acidic pHs (pH 2.0 and pH 3.5) had a less sharp decrease in peak intensity (increase in β-sheet content) with an increase in temperature. This indicates that at low concentrations the self-assembly of peptides at acidic pHs is less dependent on temperature compared to those at pH 7.0 and pH 11.0. However, at 15 mg/mL, samples at all pHs demonstrated a similar temperature dependence. In some scenarios (e.g. 15 mg/mL KF at pH 7.0 and 11.0), nearly full thermoreversible behaviour can be observed. However, for other samples (e.g. 5 and 15 mg/mL KF at pH 2.0), temperature hysteresis is identified. The different temperature dependence of secondary structure changes could be related to different peptide molecular conformations and interactions as affected by pHs and concentrations as discussed above [48]. Thermally reversible secondary structure changes have also been reported in other peptides such as MAX1, MAX2, and MAX3 [49] and a LIVAGD peptide (also named Ac-LD_6) [43]. For example, heating 150 μM MAX3 solution (125 mM Borate, 10 mM NaCl, pH 9) from 5 °C to 80 °C leads to a secondary structure conversion from random coil to β-sheet. Subsequent cooling revealed that the change is reversible [49]. Thermally reversible changes in peptide secondary structures could be rationalized by thermally triggered folding and self-assembly mainly driven by hydrophobic interactions [49,52]. Indeed, given the fact that KF peptide has three hydrophobic amino acids (Ile, Val, Leu) incorporated in positions 2, 3, 4 and 10 in which Val has a high β-sheet propensity [49], strong association of hydrophobic faces is expected during temperature-triggered self-assembly.

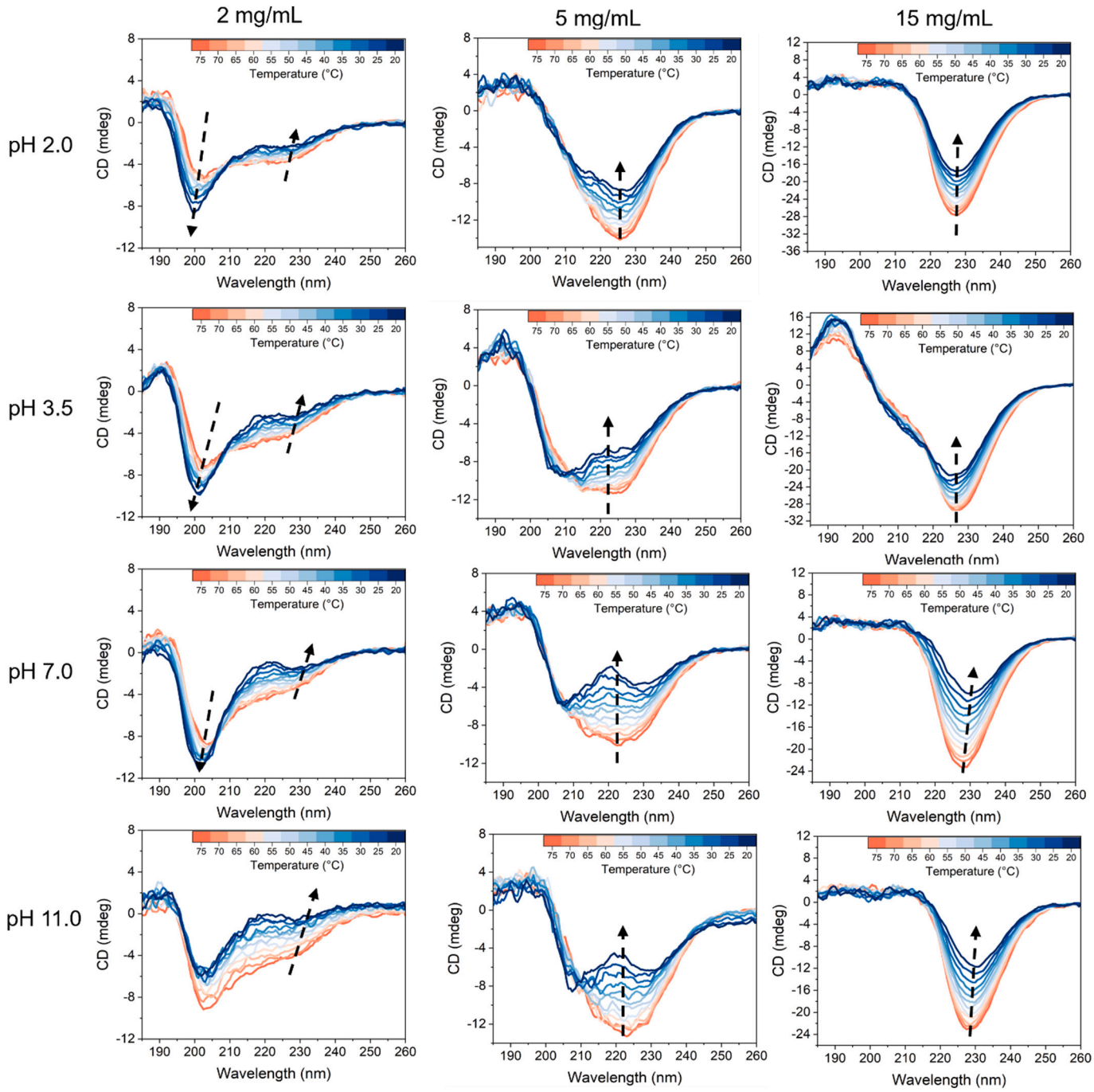

Fig. 3. Temperature-dependent CD spectra of KF peptide at various pHs (pH 2.0, pH 3.5, pH 7.0, pH 11.0) and concentrations (2 mg/mL, 5 mg/mL, and 15 mg/mL) when the temperature is decreased from 75 °C to 20 °C. Arrows indicate the CD spectra change as the temperature decreases.

3.3. Morphologies of peptide self-assembled structures as affected by pH and peptide concentration

Nanostructural characteristics of the KF peptide at various pHs and concentrations observed by TEM and micrographs are shown in Fig. 5. At 2 mg/mL, the TEM for the samples at pH 7.0 and pH 11.0 show only irregular nanoparticles without the appearance of amyloid fibrillar structures. This is consistent with the presence of disordered random coil secondary structures as revealed by CD (Fig. 1A). In contrast, the presence of extended cylindrical amyloid fibrillar structures can be observed in TEM micrographs for 2 mg/mL peptide at pH 2.0 and pH 3.5. At 5 mg/mL, the TEM for all the samples shows fibrillar structures except at pH 7.0. This could be explained by the lower content of β-sheet structures at pH 7.0 as revealed by CD (Fig. 1C). Previous studies suggested that the primary structural characteristics of amyloid fibrils are predominantly β-sheet structures [53], therefore the abundance of β-sheet structures is critical in formation of amyloid fibrils. When the concentration was increased to 15 mg/mL, nanostructures were highly dependent on pH. TEM micrographs for a sample at pH 2.0 show bundle-like structures, up to 15–20 nm thick and 100–300 nm length (Fig. 5C). The presence of these relatively large-scale bundle-like structures with extensive cross linking could contribute to the formation of a turbid hydrogel as observed in Fig. S1. TEM images for the sample at pH 3.5 clearly show the peptide self-assembled to cylindrical amyloid fibrils forming an entangled and homogenous network. Some dense clusters and bundles are formed by interactions between elongated and twisted long fibrils

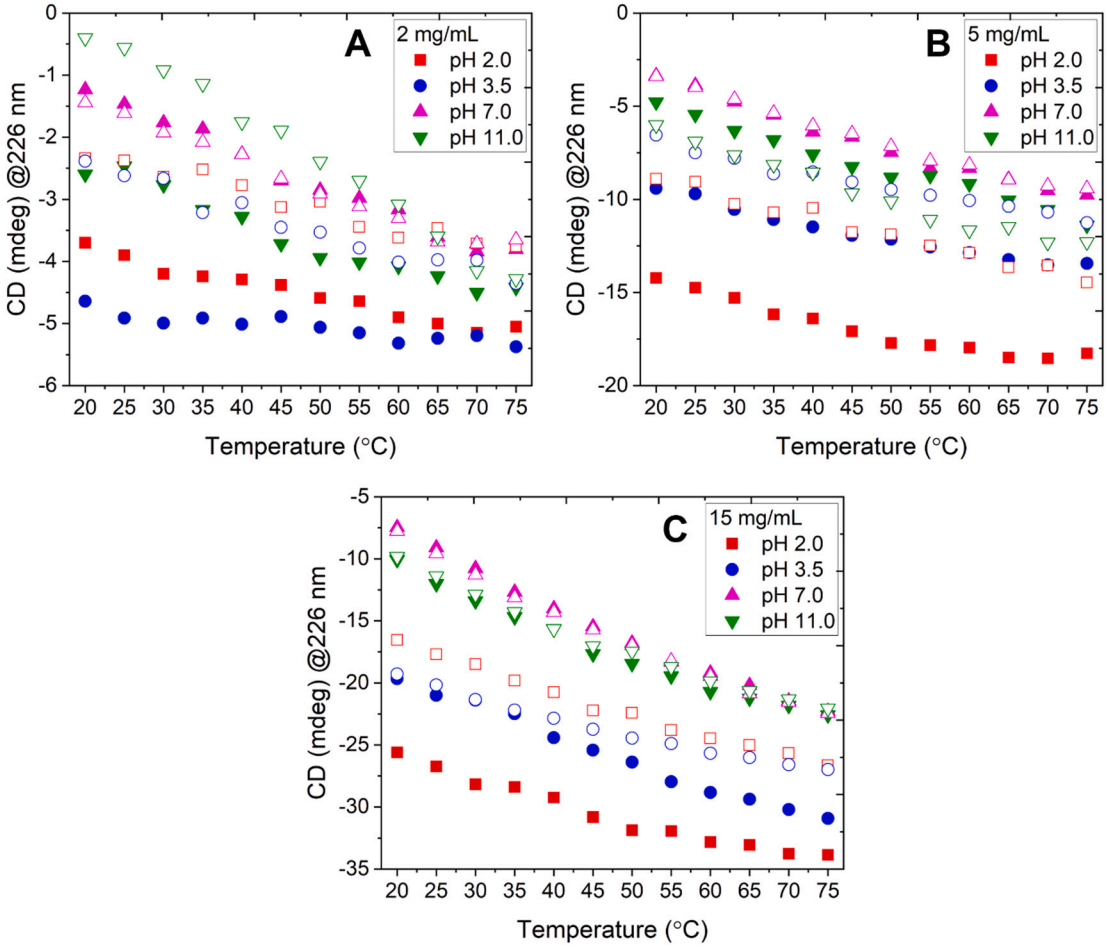

Fig. 4. Variation of the intensity of the CD negative peak at 265 nm as a function of temperature for KF peptide at (A) 2 mg/mL, (B) 5 mg/mL, and (C) 15 mg/mL. Solid and empty symbols indicate the temperature up and down measurements, respectively.

(Fig. 5F). This observation is expected as peptide hydrogels have been suggested to form by entanglement enabling the interactions of fibrils to entrap large amount of water leading to gelation [54]. This is also consistent with the observation in Fig. S1. In addition, both individual fibrils and fibril bundles can be observed. The radius of single fibrils ranges from 42.5 Å to 96.8 Å resulting in a median radius of 78.5 ± 5.0 Å. TEM images at pH 7.0 (Fig. 5I) shows the formation of globular nanospheres ranging from 10 to 20 nm in diameter that further connect to form string-like structures. These globular nanospheres could be formed due to liquid-liquid phase separation into solute-rich and solute-poor phases, leading to formations of liquid droplets [55–57]. At pH 11.0, the TEM micrographs (Fig. 5L) show the presence of extended amyloid structures with the radius of individual fibrils ranging from 55.3 Å to 88.6 Å, resulting in a median radius of 65.3 ± 7.0 Å.

Small-angle neutron scattering (SANS) experiments were conducted on the peptide at 15 mg/mL, pH 3.5 to obtain quantitative structural information on amyloid fibrils in the hydrogel state. SANS and small-angle X-ray scattering (SAXS) have been extensively used to probe nanostructures of peptide self-assembled fibrils as it can study a much greater number of nanoparticles at a time compared to microscopies thus providing more statistically representative structural information due to the volume studied [58,59]. In addition, SAXS and SANS can study peptide hydrogels in their hydrated state, thus avoiding potential structural artefacts that are induced by sample preparation for microscopies including extensive dilution, drying, and heavy metal staining [60]. The SANS profile of a 15 mg/mL sample of KF at pH 3.5 is shown in Fig. 6A along with the cylinder model fit as described in the Section 2.5. The length of peptide fibrils L is too large to be determined by the current SANS instrument set up (e.g. $L \gg Q_{min}^{-1}$, where Q_{min} is the lowest Q accessible), therefore, only radius of cylinder can be determined as 74.5 ± 4 Å (fixed standard deviation = 0.2). The obtained fibril radius correlates well with the average individual radius determined by TEM (R = 78.5 ± 5 Å). The cross-sectional radius of KF peptide fibrils is also comparable to the reported radius for the self-assembling ovalbumin peptides MMYQIGLF (~101 Å) [16] and SIINFEKL (~62 Å) [61]. In the low Q regime ($0.001 < Q$ (Å^{-1}) < 0.008), the scattering intensity I(Q) follows a power law decay I(Q) ~ Q^{-n} with a power law exponent n of 1.55, which deviates from the 'dilute' long cylinder model of $n = 1$. This could be attributed to fibril-fibril interactions and entanglement, which is confirmed by the TEM observations (Fig. 5F) [40]. Similar scattering features have been reported in previous SAXS studies from amyloid β peptide (Aβ42) fibrillar aggregates [62] and α-synuclein hydrogel [40].

3.4. Internal structure of KF amyloid fibrils as determined by X-ray diffraction (XRD)

The internal structure of KF peptide at 15 mg/mL and pH 3.5 was also studied by XRD; diffraction patterns are shown in Fig. 6B. There are two sharp reflections at 4.6 Å and 9.9 Å which has been attributed to the periodic β-strand separation and characteristic distance in the packing perpendicular to the fibril axis, respectively [63]. A minor peak at 3.8 Å corresponds to intra-β sheet features with a typical van der Waals distance of packed peptide side-chains, as reported in previous studies [64–66]. Similar XRD patterns have been reported in various self-assembling peptide systems such as coronavirus spike peptide RSAIEDLLFDKV [16] and the alternating glutamic acid/phenylalanine

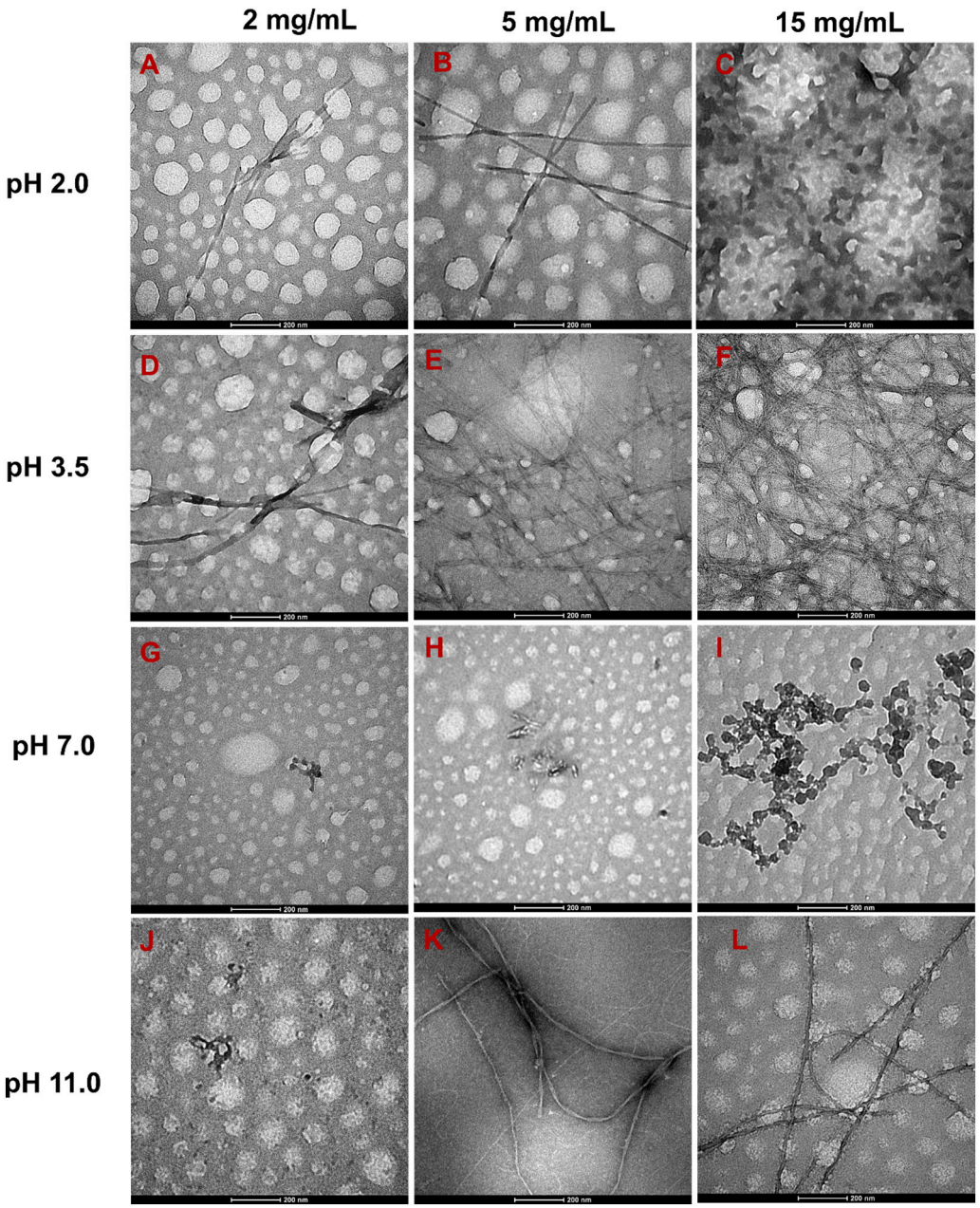

Fig. 5. TEM micrographs of KF peptide at various pHs (pH 2.0, pH 3.5, pH 7.0, pH 11.0) and concentrations (2 mg/mL, 5 mg/mL, and 15 mg/mL). Scale bar: 200 nm.

peptide (EFEFEFEF) [67].

3.5. Rheological properties of the peptide hydrogel

Rheological behaviour is one of the most critical aspects of the peptide hydrogel as it is represents a major determinant of their application in many fields such as tissue engineering, 3D printing, injectable biomaterials, etc. [68]. The small and large deformation rheological properties of the KF peptide at 15 mg/mL and pH 3.5 were determined by oscillatory rheological measurements in which storage modulus G' and loss modulus G'' were obtained. The peptide hydrogel was formed in the rheometer, and the gelation kinetics were monitored using time sweep measurements. The G' and G'' as a function of time is demonstrated in Fig. 7A. Both G' and G'' showed a steep increase with increase in gelation time up to ~200 min with the gelation kinetics subsequently slowing. The increase in elasticity is suggested to result from the formation of highly crosslinked networks with more crosslinked points [69]. After 720 min (12*h*), the gel has not reached equilibrium with G' and G'' continuously increasing over time. Similar gelation kinetics have been widely reported in other peptide hydrogels such as a bioactive peptide derived from bovine casein (FFVAPFPEVFGK) [32], peptides derived from ovalbumin (IFYCPIAIM, NIFYCPIAIM) [16], and a RATEA16 peptide [69]. It has been suggested that peptide hydrogel formation involves several steps including self-assembly into nuclei that induce formation of long fibrils, followed by further elongation, entanglement and interactions between fibrils, with subsequent structural rearrangement to form a 3D network [70]. The slow evolution of G' and G'' at longer gelation times could be explained by jamming and structural rearrangement of growing fibrils [71,72]. However, at longer gelation times, i.e., 12 h, the gelation kinetics is much slower. Therefore, frequency sweep and strain sweep measurements were conducted after 12 h of gelation.

G' and G'' as a function of frequency is shown in Fig. 7B. It can be seen that G' and G'' are nearly independent of frequency and G' is >10 fold

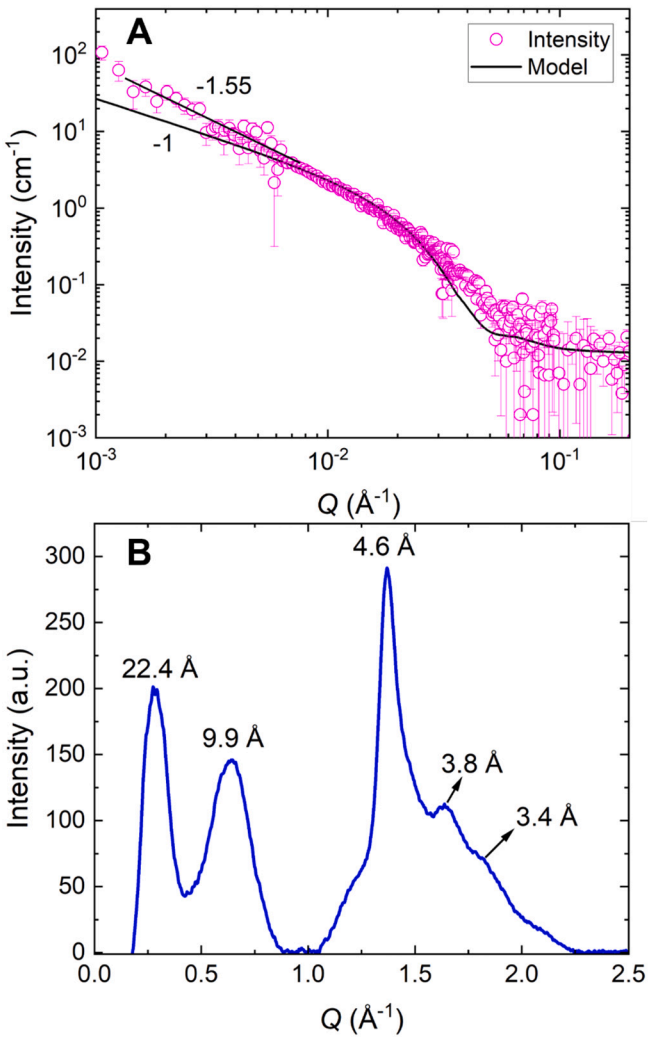

Fig. 6. (A) SANS profile of KF peptide fibrils formed at pH 3.5. The cylindrical model fit to the experimental SANS data is the solid black line. (B) X-ray diffraction (XRD) of KF peptide fibrils formed at pH 3.5.

greater than G'' in the whole frequency range, indicating the formation of a strong hydrogel with a solid-like characteristics [73]. Strain sweep data are shown in Fig. 7C. At a small strain amplitude, that is within the linear viscoelastic region (LVR), both G' and G'' are independent of strain. When the strain amplitude was increased to ~2 %, both G' and G'' declined, suggesting a structural distortion and that the gel network began to break. With a further increase in strain amplitude, a crossover of G' and G'' occurred that defines the breaking strain and breaking stress of 35 ± 3 % and ~18 ± 3 Pa, respectively. Beyond the cross over point, G'' is greater than G' suggesting the breakdown of gel network structure and that the sample started to flow [72]. The G' value at 1 Hz is 2245 ± 238 Pa. As a comparison, the G' of MAX7CNB, a 20-residue photocaged peptide is ~1000 Pa at 2 wt% (20 mg/mL); the hydrogel derived from this peptide has been applied in tissue engineering [74]. In another recent study, a self-assembled peptide (Nap-GFFKH) hydrogel with G' ~ 3000 Pa at 1 wt% has been used in drug delivery [75]. Based on previous studies, KF peptide hydrogels hold promise as a texturing agent in food and pharmaceutical products and show potential in biomedical applications such as tissue engineering and wound dressing [68].

The temperature responsive gelation behaviour of KF sample at 15 mg/mL, pH 3.5 was studied by a temperature sweep rheological measurement. The G' and G'' changes with temperature during a heating-cooling cycle is shown in Fig. 7D. During heating, both G' and G'' increased dramatically and G' increased much faster than G''. Thus, at a certain temperature, G' and G'' crossover happened and thus the gelation temperature (~30 °C) could be determined as the critical temperature where $G' = G''$. Beyond the gelation temperature, G' and G'' progressively increased with increased temperature, and G' became greater than G'', suggesting an evolution from solution state to gel state. The heating promoted hydrogelation is consistent with the CD results (Fig. 3) that heating facilitates formation of β-sheet rich protein secondary structures and consequent self-assembly. This result suggests that hydrogel formation was promoted by increasing the hydrophobic intermolecular interaction at a high temperature. Similar behaviours have been reported in previous rheological studies of a MAX3 peptide [49] and an elastin-like polypeptide [76]. In the successive cooling, the gel network is maintained, as illustrated by the continuous increase in both G' and G'' from 90 °C to ~30 °C followed by a slight decrease from ~30 °C to 20 °C. This result indicates that hydrogen bonding is also important in the hydrogel formation as the hydrogen bonding is promoted at a lower temperature. Interestingly, the expected thermoreversible gelation behaviour was not observed, although a thermoreversible change in secondary structures was observed in the CD results (Fig. 4). This could be due to annealing induced microstructural changes of peptide gel networks as reported in a previous study [77]. A detailed structural characterisation of peptide self-assembly during temperature cycling using scattering methods such as in situ synchrotron small angle X-ray scattering (SAXS) under well-controlled temperature is needed to understand the underlying mechanisms in future studies.

4. Conclusions

In this study, the self-assembly and gelation properties of a biologically active peptide KF derived from quinoa proteins was studied. The co-existence of various secondary structures and nanostructures, which are significantly affected by concentration, pH, and temperature (Fig. 8), was demonstrated. At pH 3.5 and 15 mg/mL, KF formed amyloid fibrils which interact and entangle to form a self-supporting hydrogel with G' (1 Hz) ~2300 Pa. The hydrogel formed at ~pH 3.5 makes KF a promising texturing agent for applications in acidified food products such as yoghurt [78]. Upon decreasing the pH to 2.0, an interconnected network with thicker bundles was formed. While at pH 7.0, the sample showed nanoparticles connected by strings. Concentration-dependent CD results revealed that the KF peptide at all pHs adopt a random coil conformation at low concentration (2 mg/mL) and transited to α-helix secondary structure at an intermediate concentration (5 mg/mL) except for pH 2.0 where a β-sheet rich structure was formed. Further increasing the concentration to 15 mg/mL result in all samples adopting β-sheet rich structures. Temperature also plays important role in the transitions of peptide secondary structures. Heating facilitates the conversion from random coils to α-helix at 2 mg/mL and from α-helix to β-sheet rich structures at 5 mg/mL. These findings suggest the presence of α-helical conformation in intermediate oligomeric structures during the transition between unfolded native peptide and β-sheet-rich protofibrils in amyloid fibril formation. At 15 mg/mL and all pHs, the twisted β-sheet conformation gradually transited into strong and well-defined β-sheet conformation. pH strongly affected electrostatic interactions as revealed by the self-assembly of KF peptide at pH (ca. pH 3.5) values below its isoelectric point (pI ~4.01). Increases in concentration and heat treatment enable the peptide molecules to come into closer contact through molecular crowding effect and alterations in solvation/desolvation in aqueous media, respectively [36]. This finally leads to the promotion of intermolecular H-bond and hydrophobic interactions. The π- π stacking from the F (Phenylalanine) residues may also contribute to the self-assembly and hydrogelation of the KF peptide. In summary, this study showed that peptide conformation, hydrogel formation, and nanostructure morphology can be tuned by pH, concentration, and temperature. Further studies are required to evaluate the suitability of these peptide systems for applications in food science and biomedicine.

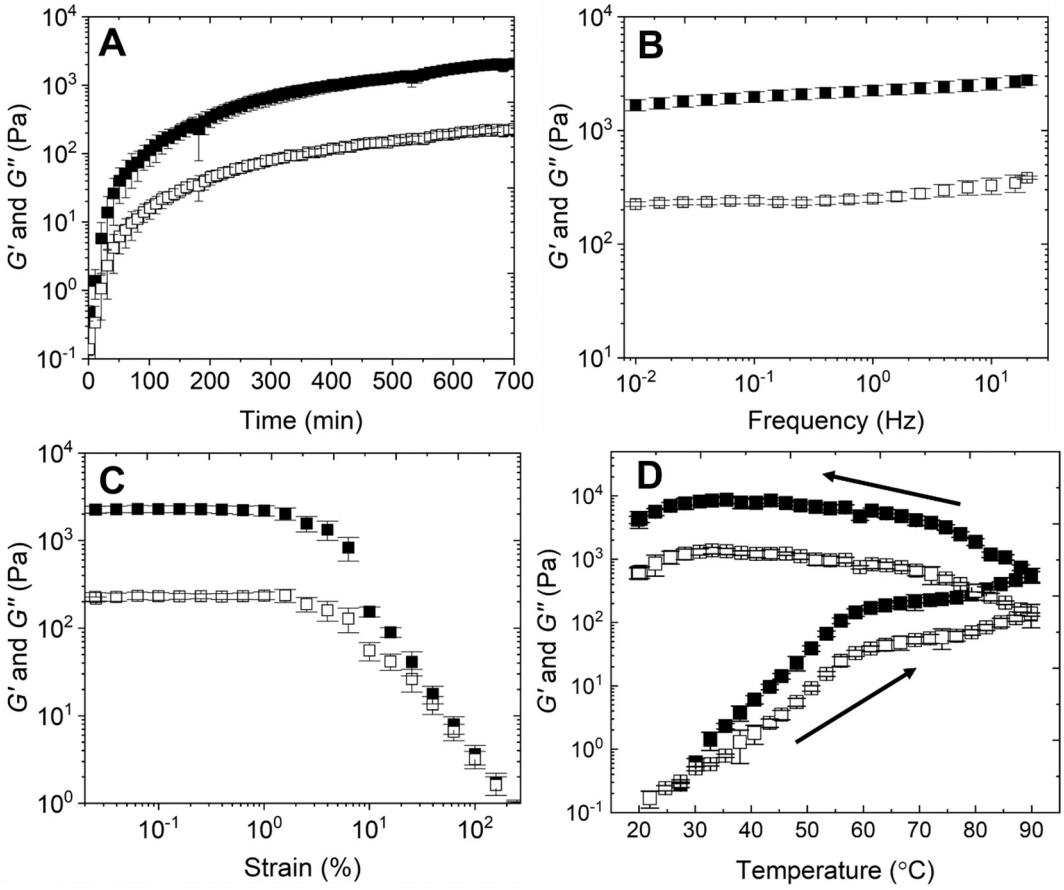

Fig. 7. The storage modulus G' and loss modulus G'' as a function of time (A), frequency (B), strain amplitude (C), and temperature (D) for KF peptide at 15 mg/mL in water, pH 3.5.

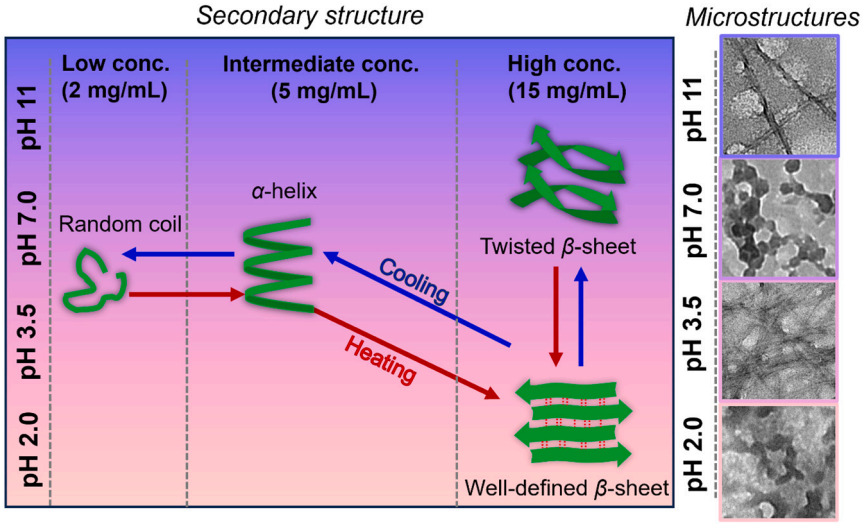

Fig. 8. Schematic representation of secondary structure and microstructural of KF peptide as regulated by concentration, pH, and temperature.

CRediT authorship contribution statement

Lirong Cheng: Writing – review & editing, Writing – original draft, Methodology, Investigation, Formal analysis, Data curation, Conceptualization. **Luis M. De Leon-Rodriguez:** Writing – review & editing, Visualization, Validation, Software, Data curation, Conceptualization. **Elliot Paul Gilbert:** Writing – review & editing, Validation, Methodology, Investigation, Formal analysis, Data curation. **Trevor Loo:** Writing – review & editing, Resources, Methodology, Data curation. **Ludwig Petters:** Writing – review & editing, Investigation, Formal analysis. **Zhi Yang:** Writing – review & editing, Writing – original draft, Visualization, Validation, Supervision, Project administration, Methodology, Investigation, Funding acquisition, Formal analysis, Data curation, Conceptualization.

Declaration of competing interest

The authors declare that there is no conflict interest in this study.

Data availability

Data will be made available on request.

Acknowledgements

This work was funded by the College of Sciences Massey University Research Fund (MURF) (RM 24956) to Early Career Researchers (Z.Y.). We appreciate the discussion with Dr. Yacine Hemar during the early stage of this project, and Ms. Ruijia Zhang for preliminary gelation screening experiments, and the technical support from Dr. Yanyu He (Manawatu Microscopy and Imaging Centre) for technical support on TEM imaging. The authors acknowledge the support of the Australian Centre for Neutron Scattering, ANSTO in supporting the QUOKKA neutron research infrastructure used in this work via ACNS proposal P15802.

Appendix A. Supplementary data

Supplementary data to this article can be found online at https://doi.org/10.1016/j.ijbiomac.2024.129296.

References

[1] J. Wang, K. Liu, R. Xing, X. Yan, Peptide self-assembly: thermodynamics and kinetics, Chem. Soc. Rev. 45 (20) (2016) 5589–5604.
[2] J.-P.S. Powers, R.E. Hancock, The relationship between peptide structure and antibacterial activity, Peptides 24 (11) (2003) 1681–1691.
[3] H. Chen, T. Zhang, Y. Tian, L. You, Y. Huang, S. Wang, Novel self-assembling peptide hydrogel with pH-tunable assembly microstructure, gel mechanics and the entrapment of curcumin, Food Hydrocoll. 124 (2022) 107338.
[4] N.F. Theodoroula, C. Karavasili, M.C. Vlasiou, A. Primikyri, C. Nicolaou, A. V. Chatzikonstantinou, A.-T. Chatzitaki, C. Petrou, N. Bouropoulos, C.K. Zacharis, E. Galatou, Y. Sarigiannis, D.G. Fatouros, I.S. Vizirianakis, NGIWY-amide: a bioinspired ultrashort self-assembled peptide Gelator for local drug delivery applications, Pharmaceutics 14 (1) (2022) 133.
[5] R. Pugliese, F. Gelain, Characterization of elastic, thermo-responsive, self-healable supramolecular hydrogel made of self-assembly peptides and guar gum, Mater. Des. 186 (2020) 108370.
[6] J.D. Tang, C. Mura, K.J. Lampe, Stimuli-responsive, pentapeptide, nanofiber hydrogel for tissue engineering, J. Am. Chem. Soc. 141 (12) (2019) 4886–4899.
[7] D.J. Adams, Personal perspective on understanding low molecular weight gels, J. Am. Chem. Soc. 144 (25) (2022) 11047–11053.
[8] J.K. Gupta, D.J. Adams, N.G. Berry, Will it gel? Successful computational prediction of peptide gelators using physicochemical properties and molecular fingerprints, Chemical Science 7 (7) (2016) 4713–4719.
[9] T. Xu, J. Wang, S. Zhao, D. Chen, H. Zhang, Y. Fang, N. Kong, Z. Zhou, W. Li, H. Wang, Accelerating the prediction and discovery of peptide hydrogels with human-in-the-loop, Nat. Commun. 14 (1) (2023) 3880.
[10] R. Pugliese, M. Bartolomei, C. Bollati, G. Boschin, A. Arnoldi, C. Lammi, Gel-forming of self-assembling peptides functionalized with food bioactive motifs modulate DPP-IV and ACE inhibitory activity in human intestinal Caco-2 cells, Biomedicines 10 (2) (2022) 330.
[11] A. Vahedifar, J. Wu, Self-assembling peptides: structure, function, in silico prediction and applications, Trends Food Sci. Technol. 119 (2022) 476–494.
[12] L.M. De Leon Rodriguez, Y. Hemar, Prospecting the applications and discovery of peptide hydrogels in food, Trends Food Sci. Technol. 104 (2020) 37–48.
[13] H. Chen, X. Cai, J. Cheng, S. Wang, Self-assembling peptides: molecule-nanostructure-function and application on food industry, Trends Food Sci. Technol. 120 (2022) 212–222.
[14] M. Akbarian, A. Khani, S. Eghbalpour, V.N. Uversky, Bioactive peptides: synthesis, sources, applications, and proposed mechanisms of action, Int. J. Mol. Sci. 23 (3) (2022) 1445.
[15] D. Doucet, E.A. Foegeding, Gel formation of peptides produced by extensive enzymatic hydrolysis of β-Lactoglobulin, Biomacromolecules 6 (2) (2005) 1140–1148.
[16] R.O. Abioye, C. Acquah, P.C.Q. Hsu, N. Hüttmann, X. Sun, C.C. Udenigwe, Self-assembly and hydrogelation properties of peptides derived from peptic cleavage of aggregation-prone regions of ovalbumin, Gels 8 (10) (2022) 641.
[17] L. Josefsson, X. Ye, C.J. Brett, J. Meijer, C. Olsson, A. Sjögren, J. Sundlöf, A. Davydok, M. Langton, Å. Emmer, C. Lendel, Potato protein nanofibrils produced from a starch industry sidestream, ACS Sustain. Chem. Eng. 8 (2) (2020) 1058–1067.
[18] R. Pugliese, A. Arnoldi, C. Lammi, Nanostructure, self-assembly, mechanical properties, and antioxidant activity of a lupin-derived peptide hydrogel, Biomedicines 9 (3) (2021) 294.
[19] A.-M. Fernandez-Escamilla, F. Rousseau, J. Schymkowitz, L. Serrano, Prediction of sequence-dependent and mutational effects on the aggregation of peptides and proteins, Nat. Biotechnol. 22 (10) (2004) 1302–1306.
[20] N. Louros, K. Konstantoulea, M. De Vleeschouwer, M. Ramakers, J. Schymkowitz, F. Rousseau, WALTZ-DB 2.0: an updated database containing structural information of experimentally determined amyloid-forming peptides, Nucleic Acids Res. 48 (D1) (2020) D389–D393.
[21] L. Luo, L. Cheng, R. Zhang, Z. Yang, Impact of high-pressure homogenization on physico-chemical, structural, and rheological properties of quinoa protein isolates, Food Struct. 32 (2022) 100265.
[22] P. Mudgil, B.P. Kilari, H. Kamal, O.A. Olalere, R.J. FitzGerald, C.-Y. Gan, S. Maqsood, Multifunctional bioactive peptides derived from quinoa protein hydrolysates: inhibition of α-glucosidase, dipeptidyl peptidase-IV and angiotensin I converting enzymes, J. Cereal Sci. 96 (2020) 103130.
[23] X. Fan, H. Guo, A. Richel, L. Zhang, C. Liu, P. Qin, C. Blecker, G. Ren, Preparation, physicochemical properties, and formation mechanism of quinoa self-assembled peptide-based hydrogel, Food Hydrocoll. 145 (2023) 109139.
[24] V. Castelletto, I.W. Hamley, Amyloid and hydrogel formation of a peptide sequence from a coronavirus spike protein, ACS Nano 16 (2) (2022) 1857–1867.
[25] F. Rousseau, J. Schymkowitz, L. Serrano, Protein aggregation and amyloidosis: confusion of the kinds? Curr. Opin. Struct. Biol. 16 (1) (2006) 118–126.
[26] R. Linding, J. Schymkowitz, F. Rousseau, F. Diella, L. Serrano, A comparative study of the relationship between protein structure and β-aggregation in globular and intrinsically disordered proteins, J. Mol. Biol. 342 (1) (2004) 345–353.
[27] J.C. Schulz Gilbert, T.J. Noakes, 'Quokka'—the small-angle neutron scattering instrument at OPAL, Phys. B Condens. Matter 385 (2006) 1180–1182.
[28] K. Wood, J.P. Mata, C.J. Garvey, C.-M. Wu, W.A. Hamilton, P. Abbeywick, D. Bartlett, F. Bartsch, P. Baxter, N. Booth, QUOKKA, the pinhole small-angle neutron scattering instrument at the OPAL research reactor, Australia: design, performance, operation and scientific highlights, J. Appl. Cryst. 51 (2) (2018) 294–314.
[29] J. Ilavsky, P.R. Jemian, Irena: tool suite for modeling and analysis of small-angle scattering, J. Appl. Cryst. 42 (2) (2009) 347–353.
[30] G. Fournet, A. Guinier, Small angle scattering of X-rays, translated by Walker, CB and Yudowitch, KL In: New York: John Wiley & Sons (1955) 7–78.
[31] F. Zhang, F. Roosen-Runge, M.W. Skoda, R.M. Jacobs, M. Wolf, P. Callow, H. Frielinghaus, V. Pipich, S. Prevost, F. Schreiber, Hydration and interactions in protein solutions containing concentrated electrolytes studied by small-angle scattering, Phys. Chem. Chem. Phys. 14 (7) (2012) 2483–2493.
[32] N. Petit, J.M. Dyer, J.A. Gerrard, L.J. Domigan, S. Clerens, Insight into the self-assembly and gel formation of a bioactive peptide derived from bovine casein, BBA Advances 3 (2023) 100086.
[33] M.S. Haines, E. Ramirez, K.B.E. Moore, J.S. Fortin, Revisiting misfolding propensity of serum amyloid A1: special focus on the signal peptide region, Biochemistry and Biophysics Reports 31 (2022) 101284.
[34] M.J. Krysmann, V. Castelletto, A. Kelarakis, I.W. Hamley, R.A. Hule, D.J. Pochan, Self-assembly and hydrogelation of an amyloid peptide fragment, Biochemistry 47 (16) (2008) 4597–4605.
[35] M. Krysmann, V. Castelletto, J. McKendrick, L. Clifton, P. Harris, S. King, Self-assembly of peptide nanotubes in an organic solvent, Langmuir 24 (15) (2008) 8158–8162.
[36] G. Ghosh, R. Barman, A. Mukherjee, U. Ghosh, S. Ghosh, G. Fernández, Control over multiple nano- and secondary structures in peptide self-assembly, Angew. Chem. Int. Ed. 61 (5) (2022) e202113403.
[37] P.C. Ke, R. Zhou, L.C. Serpell, R. Riek, T.P. Knowles, H.A. Lashuel, E. Gazit, I. W. Hamley, T.P. Davis, M. Fändrich, Half a century of amyloids: past, present and future, Chem. Soc. Rev. 49 (15) (2020) 5473–5509.
[38] I.W. Hamley, The amyloid beta peptide: a chemist's perspective. Role in Alzheimer's and fibrillization, Chemical Reviews 112 (10) (2012) 5147–5192.
[39] T. Li, X.-M. Lu, M.-R. Zhang, K. Hu, Z. Li, Peptide-based nanomaterials: self-assembly, properties and applications, Bioactive Materials 11 (2022) 268–282.
[40] B.H. Pogostin, S. Linse, U. Olsson, Fibril charge affects α-synuclein hydrogel rheological properties, Langmuir 35 (50) (2019) 16536–16544.
[41] C. Avitabile, L.D. D'Andrea, A. Romanelli, Circular dichroism studies on the interactions of antimicrobial peptides with bacterial cells, Sci. Rep. 4 (1) (2014) 4293.
[42] C.S. Starck, A.J. Sutherland-Smith, Cytotoxic aggregation and amyloid formation by the myostatin precursor protein, PloS One 5 (2) (2010) e9170.
[43] C.A. Hauser, R. Deng, A. Mishra, Y. Loo, U. Khoe, F. Zhuang, D.W. Cheong, A. Accardo, M.B. Sullivan, C. Riekel, Natural tri-to hexapeptides self-assemble in water to amyloid β-type fiber aggregates by unexpected α-helical intermediate structures, Proc. Natl. Acad. Sci. 108 (4) (2011) 1361–1366.
[44] I. Seim, A.E. Posey, W.T. Snead, B.M. Stormo, D. Klotsa, R.V. Pappu, A. S. Gladfelter, Dilute phase oligomerization can oppose phase separation and modulate material properties of a ribonucleoprotein condensate, Proc. Natl. Acad. Sci. 119 (13) (2022) e2120799119.
[45] C. Diaferia, F. Netti, M. Ghosh, T. Sibillano, C. Giannini, G. Morelli, L. Adler-Abramovich, A. Accardo, Bi-functional peptide-based 3D hydrogel-scaffolds, Soft Matter 16 (30) (2020) 7006–7017.
[46] A. Abedini, D.P. Raleigh, A role for helical intermediates in amyloid formation by natively unfolded polypeptides? Phys. Biol. 6 (1) (2009) 015005.
[47] S. Kumar, S.K. Mohanty, J.B. Udgaonkar, Mechanism of formation of amyloid protofibrils of barstar from soluble oligomers: evidence for multiple steps and

lateral association coupled to conformational conversion, J. Mol. Biol. 367 (4) (2007) 1186–1204.
[48] M. Cao, Y. Shen, Y. Wang, X. Wang, D. Li, Self-assembly of short elastin-like amphiphilic peptides: effects of temperature, molecular hydrophobicity and charge distribution, Molecules 24 (1) (2019) 202.
[49] D.J. Pochan, J.P. Schneider, J. Kretsinger, B. Ozbas, K. Rajagopal, L. Haines, Thermally reversible hydrogels via intramolecular folding and consequent self-assembly of a de novo designed peptide, J. Am. Chem. Soc. 125 (39) (2003) 11802–11803.
[50] L.M. De Leon-Rodriguez, Y. Hemar, G. Mo, A.K. Mitra, J. Cornish, M.A. Brimble, Multifunctional thermoresponsive designer peptide hydrogels, Acta Biomater. 47 (2017) 40–49.
[51] Y. Liu, Y. Yang, C. Wang, X. Zhao, Stimuli-responsive self-assembling peptides made from antibacterial peptides, Nanoscale 5 (14) (2013) 6413–6421.
[52] K. Rajagopal, B. Ozbas, D.J. Pochan, J.P. Schneider, Probing the importance of lateral hydrophobic association in self-assembling peptide hydrogelators, Eur. Biophys. J. 35 (2006) 162–169.
[53] B.H. Toyama, J.S. Weissman, Amyloid structure: conformational diversity and consequences, Annu. Rev. Biochem. 80 (1) (2011) 557–585.
[54] K. Medini, B.W. Mansel, M.A. Williams, M.A. Brimble, D.E. Williams, J.A. Gerrard, Controlling gelation with sequence: towards programmable peptide hydrogels, Acta Biomater. 43 (2016) 30–37.
[55] C. Yuan, A. Levin, W. Chen, R. Xing, Q. Zou, T.W. Herling, P.K. Challa, T.P. J. Knowles, X. Yan, Nucleation and growth of amino acid and peptide supramolecular polymers through liquid–liquid phase separation, Angew. Chem. Int. Ed. 58 (50) (2019) 18116–18123.
[56] P. Zhou, R. Xing, Q. Li, J. Li, C. Yuan, X. Yan, Steering phase-separated droplets to control fibrillar network evolution of supramolecular peptide hydrogels, Matter 6 (6) (2023) 1945–1963.
[57] C. Yuan, Q. Li, R. Xing, J. Li, X. Yan, Peptide self-assembly through liquid-liquid phase separation, Chem 9 (9) (2023) 2425–2445.
[58] J. Li, Y. Zhao, P. Zhou, X. Hu, D. Wang, S.M. King, S.E. Rogers, J. Wang, J.R. Lu, H. Xu, Ordered nanofibers fabricated from hierarchical self-assembling processes of designed α-helical peptides, Small 16 (45) (2020) 2003945.
[59] J.-B. Guilbaud, A. Saiani, Using small angle scattering (SAS) to structurally characterise peptide and protein self-assembled materials, Chem. Soc. Rev. 40 (3) (2011) 1200–1210.
[60] L. de Campo Yang, E.P. Gilbert, R. Knott, L. Cheng, B. Storer, X. Lin, L. Luo, S. Patole, Y. Hemar, Effect of NaCl and $CaCl_2$ concentration on the rheological and structural characteristics of thermally-induced quinoa protein gels, Food Hydrocoll. 124 (2022) 107350.
[61] M. Kamalov, H. Kählig, C. Rentenberger, A.R.M. Müllner, H. Peterlik, C.F. W. Becker, Ovalbumin epitope SIINFEKL self-assembles into a supramolecular hydrogel, Sci. Rep. 9 (1) (2019) 2696.
[62] V. Lattanzi, I. André, U. Gasser, M. Dubackic, U. Olsson, S. Linse, Amyloid β 42 fibril structure based on small-angle scattering, Proc. Natl. Acad. Sci. 118 (48) (2021) e2112783118.
[63] L.C. Serpell, Alzheimer's amyloid fibrils: structure and assembly, Biochimica et Biophysica Acta (BBA)-Molecular Basis of Disease 1502 (1) (2000) 16–30.
[64] M. Sunde, L.C. Serpell, M. Bartlam, P.E. Fraser, M.B. Pepys, C.C.F. Blake, Common core structure of amyloid fibrils by synchrotron X-ray diffraction. Edited by F. E. Cohen, Journal of Molecular Biology 273 (3) (1997) 729–739.
[65] I.W. Hamley, A. Dehsorkhi, V. Castelletto, J. Seitsonen, J. Ruokolainen, H. Iatrou, Self-assembly of a model amphiphilic oligopeptide incorporating an arginine headgroup, Soft Matter 9 (19) (2013) 4794–4801.
[66] M.F. Perutz, J.T. Finch, J. Berriman, A. Lesk, Amyloid fibers are water-filled nanotubes, Proc. Natl. Acad. Sci. 99 (8) (2002) 5591–5595.
[67] L.R. Mello, I.W. Hamley, A. Miranda, W.A. Alves, E.R. Silva, β-Sheet assembly in amyloidogenic glutamic acid nanostructures: insights from X-ray scattering and infrared nanospectroscopy, J. Pept. Sci. 25 (6) (2019) e3170.
[68] L.M.D.L. Rodriguez, Y. Hemar, J. Cornish, M.A. Brimble, Structure–mechanical property correlations of hydrogel forming β-sheet peptides, Chem. Soc. Rev. 45 (17) (2016) 4797–4824.
[69] Y. Zhao, H. Yokoi, M. Tanaka, T. Kinoshita, T. Tan, Self-assembled pH-responsive hydrogels composed of the RATEA16 peptide, Biomacromolecules 9 (6) (2008) 1511–1518.
[70] L.J. Thursch, D. DiGuiseppi, T.R. Lewis, R. Schweitzer-Stenner, N.J. Alvarez, Exploring the gel phase of cationic glycylalanylglycine in ethanol/water. I. Rheology and microscopy studies, J. Colloid Interface Sci. 564 (2020) 499–509.
[71] R. Schweitzer-Stenner, N.J. Alvarez, Short peptides as tunable, switchable, and strong gelators, J. Phys. Chem. B. 125 (25) (2021) 6760–6775.
[72] Z. Yang, Y. Hemar, L. Hilliou, E.P. Gilbert, D.J. McGillivray, M.A.K. Williams, S. Chaieb, Nonlinear behavior of gelatin networks reveals a hierarchical structure, Biomacromolecules 17 (2) (2016) 590–600.
[73] C. Yan, D.J. Pochan, Rheological properties of peptide-based hydrogels for biomedical and other applications, Chem. Soc. Rev. 39 (9) (2010) 3528–3540.
[74] L.A. Haines, K. Rajagopal, B. Ozbas, D.A. Salick, D.J. Pochan, J.P. Schneider, Light-activated hydrogel formation via the triggered folding and self-assembly of a designed peptide, J. Am. Chem. Soc. 127 (48) (2005) 17025–17029.
[75] T. Cui, X. Li, S. He, D. Xu, L. Yin, X. Huang, S. Deng, W. Yue, W. Zhong, Instant self-assembly peptide hydrogel encapsulation with fibrous alginate by microfluidics for infected wound healing, ACS Biomater Sci. Eng. 6 (9) (2020) 5001–5011.
[76] Y. Mizuguchi, Y. Mashimo, M. Mie, E. Kobatake, Temperature-responsive multifunctional protein hydrogels with elastin-like polypeptides for 3-D angiogenesis, Biomacromolecules 21 (3) (2020) 1126–1135.
[77] Q. Li, G. Zhang, Y. Wu, Y. Wang, Y. Liang, X. Yang, W. Qi, R. Su, Z. He, Control of peptide hydrogel formation and stability via heating treatment, J. Colloid Interface Sci. 583 (2021) 234–242.
[78] R. Gyawali, S.A. Ibrahim, Effects of hydrocolloids and processing conditions on acid whey production with reference to Greek yogurt, Trends Food Sci. Technol. 56 (2016) 61–76.